Journal of
Materials Chemistry B

ROYAL SOCIETY OF CHEMISTRY

COMMUNICATION

View Article Online
View Journal | View Issue

Cite this: *J. Mater. Chem. B*, 2026, **14**, 5238

Received 5th December 2025, Accepted 7th April 2026

DOI: 10.1039/d5tb02723c

rsc.li/materials-b

Influence of liquid repellency and slipperiness on blood-material interactions

Halle J. Cantor, †[ab] Adil Rather,†[cd] Ragavi Rajasekaran, [c] Adrian Aligwekwe,[ab] Ashley C. Brown *[ab] and Arun Kumar Kota *[c]

Blood-contacting medical devices are an integral part of modern medicine, but as a foreign material, the immune system is inherently activated and induces thrombosis. To avoid the adverse effects of the devices, concurrent anticoagulant therapies are frequently administered, but anticoagulants carry their own detrimental risks. Therefore, we investigated the interactions of blood cells with non-textured surfaces on glass coverslips functionalized with polymeric brushes. We synthesized four categories of distinct surface coatings and characterized them based on liquid repellency and slipperiness: less slippery hydrophobic, more slippery hydrophobic, less slippery hydrophilic, and more slippery hydrophilic. Fluorescent imaging revealed that platelets and leukocytes adhere and activate significantly less on the more slippery hydrophilic (SLIC) surfaces compared to the other three surfaces. Microfluidics coupled with fluorescent microscopy showed that under dynamic conditions with an actively polymerizing flow buffer, the SLIC-coated glass not only inhibited clot growth, but also enabled clot degradation compared to uncoated glass. This work demonstrates the potential of SLIC surfaces in reducing adverse thrombotic events resulting from blood-contacting medical devices.

1. Introduction

Blood-contacting medical implants and devices (*e.g.*, vascular grafts, stents, heart valves, left ventricular assist devices, heart-lung machines, *etc.*) have saved or improved the quality of life for millions of patients.[1,2] Despite their widespread use, all blood-contacting implants and devices have been shown to initiate inflammation, hemolysis, platelet activation, fibrosis, and/or infection, potentially leading to long-term complications.[3–5] As a result, these implants and devices typically require anticoagulants and sometimes antiplatelet therapies, posing off-target bleeding risks and costs to the patient.[2,6,7] The initial contact of blood with a foreign surface triggers the rapid adsorption of plasma proteins such as fibrinogen, which facilitates platelet and leukocyte adhesion and platelet activation, leading to initiation of the coagulation cascade and thrombosis.[5,8] Therefore, surface modifications that modulate blood-material interactions to minimize thrombosis are highly desirable. In recent years, slippery surfaces – characterized by their ability to promote high liquid droplet mobility – have garnered significant interest for a variety of biofluidic applications, including the minimization of thrombosis.[9,10] Broadly, slippery surfaces can be classified into three categories based on their underlying mechanism of inducing slipperiness: (i) textured super-repellent surfaces, (ii) textured lubricant-infused surfaces, and (iii) non-textured, liquid-like surfaces functionalized with polymeric brushes. Super-repellent surfaces achieve slipperiness by combining surface texture with trapped air.[11,12] Liquid-infused surfaces attain slipperiness by combining surface texturing with trapped immiscible liquid lubricant.[13,14] However, both of these textured systems often suffer from durability challenges, such as damage to surface texture or depletion of trapped air or lubricant, leading to compromised performance over time.[15–18] To overcome these limitations, non-textured, liquid-like surfaces functionalized with covalently grafted oligomeric or polymeric brushes have emerged as promising alternatives.[7,19–23] These liquid-like surfaces are characterized by dynamic mobility and conformational flexibility of the grafted molecular chains, which enable low resistance to droplet motion while avoiding texture-related degradation mechanisms.[19–22] However, the majority of such surfaces reported to date have been hydrophobic in nature.[18,23–27] Hydrophobic surfaces tend to adsorb blood proteins strongly and promote platelet adhesion and activation, thereby increasing the risk of thrombotic events.[28–31] In contrast, we recently reported the systematic design

---

[a] Lampe Joint Department of Biomedical Engineering, North Carolina State University and University of North Carolina at Chapel Hill, Raleigh, NC 27695, USA. E-mail: aecarso2@ncsu.edu

[b] Comparative Medicine Institute, North Carolina State University, Raleigh, NC 27606, USA

[c] Department of Mechanical and Aerospace Engineering, North Carolina State University, Raleigh 27606, USA. E-mail: akota2@ncsu.edu

[d] Department of Chemistry, National Institute of Technology, Srinagar, 190006, India

† Equal contribution.

of a novel class of non-textured, liquid-like slippery hydrophilic (SLIC) surfaces.[32] These materials exhibit an unconventional combination of surface properties: water droplets spread easily, indicating hydrophilicity, yet slide off readily, demonstrating slipperiness. This arguably counterintuitive behavior challenges traditional assumptions that hydrophilic surfaces inherently promote strong droplet pinning, resulting in poor mobility. In our recent work, we observed that SLIC surfaces can not only delay fibrinogen adsorption, but also hinder platelet adhesion and activation, suggesting a unique ability to modulate early blood-material interactions.[33–35]

Wetting is commonly characterized by two distinct measures – contact angle (a measure of liquid repellency) and slipperiness *via* sliding angle or contact angle hysteresis (a measure of droplet mobility).[36,37] In this study, liquid repellency is defined based on the static contact angles, where hydrophobic surfaces display contact angle $\theta > 90^\circ$ and hydrophilic surfaces display $\theta < 90^\circ$. Surface slipperiness is defined based on sliding angles, where sliding angle $\omega < 10^\circ$ indicates high slipperiness and $\omega \gg 10^\circ$ indicates strong pinning. Note that the sliding angle is an inverse measure of slipperiness. While many studies have investigated how liquid repellency (contact angle) affects protein adsorption and thrombus formation, the independent role of slipperiness (sliding angle or contact angle hysteresis) has not been investigated. This distinction is important because surface slipperiness reduces contact line pinning and promotes droplet mobility, which in turn may influence protein adsorption as well as the adhesion and activation of blood cells, thereby controlling thrombosis on blood-contacting surfaces. To better understand the independent roles of liquid repellency (*i.e.*, hydrophilic *vs.* hydrophobic surfaces) and slipperiness (*i.e.*, less slippery *vs.* more slippery surfaces) on blood-material interactions, in this work, we fabricated four distinct types of surfaces – less slippery hydrophobic, more slippery hydrophobic, less slippery hydrophilic, and more slippery hydrophilic – each exhibiting controlled combinations of wettability and slipperiness. We assessed platelet and leukocyte adhesion and activation as a function of liquid repellency and slipperiness, while being intentionally agnostic to other surface properties (*e.g.*, surface mechanical properties, surface charge, surface chemistry *etc.*). Our findings demonstrate that while slipperiness is critical for reducing cellular adhesion, hydrophilicity is a key co-factor for minimizing adverse blood-material interactions. These insights provide a mechanistic understanding of how surface properties influence thromboresistance. Our work offers fundamental insights for the design of advanced blood-contacting biomaterials, highlighting the importance of SLIC surfaces (emerging class of surfaces), which combine hydrophilicity and slipperiness, for reducing thrombosis in cardiovascular and extracorporeal medical devices.

2. Experimental section

2.1. Fabrication of different surfaces

To fabricate the hydrophobic and hydrophilic surfaces, 12 mm round glass coverslips (Fisher) were washed thoroughly with deionized water and isopropanol (Fisher) sequentially, and then dried with nitrogen. The precleaned surfaces were exposed to oxygen plasma (Plasma Etch PE-25) for 10 minutes for hydroxylation prior to chemical modification. Note that less slippery hydrophilic surfaces were washed cover slips, without plasma-treatment. To fabricate less slippery hydrophobic surfaces, the hydroxylated surfaces were exposed to the vapors of 200 μL of heptadecafluoro-1,1,2,2-tetrahydrodecyl trichlorosilane (Gelest) in an enclosed chamber for 60 minutes at 120 °C. To fabricate more slippery hydrophobic surfaces, the hydroxylated glass surfaces were exposed to the vapors of 150 μL of 1,3-dichlorotetramethyldisiloxane (Gelest) in an enclosed chamber for 15 minutes at room temperature. To fabricate more slippery hydrophilic surfaces, the hydroxylated glass surfaces were immersed in a solution of PEG silane 3-[methoxy-(polyethyleneoxy)9-12] propyltrimethoxysilane (Gelest; 6 μL), hydrochloric acid (Fisher; 12 μL), and anhydrous toluene (Fisher; 40 mL) for 5 hours at room temperature. Finally, all the silanized samples were cleaned by rinsing thoroughly with anhydrous toluene, DI water, and isopropanol sequentially, and then dried with nitrogen.

2.2. Characterization of surface wettability

The surface wettability (liquid repellency and slipperiness) of different surfaces was characterized using contact angle goniometry (Ramé-Hart 260-F4). Static contact angles were measured by depositing a small volume of liquid (20 μL) on the surface. Sliding angles were measured by slowly tilting the stage until the droplet started sliding. All measurements were performed at ambient laboratory conditions in room temperature. All results are reported as the mean ± standard deviation of three independent measurements.

2.3. Characterization of surface chemistry

The surface chemistry on all four surfaces was characterized using Attenuated Total Reflectance Fourier Transform Infrared (ATR-FTIR) spectroscopy (Thermo Scientific Nicolet iS50 spectrometer). Spectra were acquired at a resolution of 2 cm^{-1}, averaging 500 scans per sample. Background spectra were obtained using an empty ATR crystal and subtracted from the uncoated sample spectra using the instrument software.

2.4. Characterization of surface topography

Topography maps and root mean square surface roughness measurements for all four surfaces were characterized using a confocal laser scanning microscope (Keyence VKx1100), which combines optical microscopy with laser profilometry.

2.5. Estimation of surface energy

Surface free energy of all four surfaces was quantified using the Owens-Wendt approach based on contact angle measurements with polar and non-polar liquids (see Supporting Information (SI), Section S1).

2.6. Characterization of protein adsorption

Each surface was immersed in bovine serum albumin (BSA, Thermo Fisher; 1 mg mL^{-1}) or fibrinogen (Fib, Thermo Fisher; 1 mg mL^{-1}) solutions and incubated for 2 h, 6 h, 24 h and 48 h to enable time-resolved adsorption profiling. At each time point, samples were removed and gently rinsed with phosphate-buffered saline (PBS, Thermo Fisher; pH 7.4) to remove free or loosely bound protein. Protein adsorption of BSA and Fib was then quantified using a bicinchoninic acid (BCA) protein assay kit (Thermo Fisher), prepared and used according to the manufacturer's instructions. The BSA standard curve was generated by measuring the absorbance at 562 nm for a series of known BSA concentrations (0.0075–2 mg mL^{-1}). Linear regression was performed to obtain the best-fit line and correlation coefficient. The absorbance values of all samples were then converted to protein amounts by interpolating from the standard curve, and the adsorbed protein per surface was calculated accordingly. All protein adsorption measurements were performed in triplicate, and the reported values represent the mean ± standard deviation.

2.7. Isolation of human blood cells

Healthy pathogen-screened human whole blood was purchased from a commercial source in acid-citrate dextrose (ZenBio, Inc). Whole blood was returned to room temperature prior to centrifuging for 15 minutes at 150*g* to collect platelet-rich plasma. The remaining leukocytes and red blood cells (RBCs) were gently resuspended with 1× RBC lysis buffer (Invitrogen, 00-4333-57) and placed on a rocker protected from light for 10 minutes. The suspension of leukocytes and lysed RBCs were then centrifuged for 5 minutes at 350*g* to allow pelleting of leukocytes. Platelet-rich plasma was further centrifuged for 5 minutes at 900*g* to allow pelleting of platelets. Leukocytes and platelets were gently resuspended in 1× phosphate buffered saline (PBS) to the original blood volume.

2.8. Characterization of blood cell adhesion and activation assays

Glass coverslips were coated with 1% BSA in 1× PBS for negative controls or with 3 mg mL^{-1} purified human fibrinogen for positive controls at 4 °C overnight. All coverslips were then washed with 1× PBS, platelets or leukocytes were added, and the cells were allowed to incubate at room temperature for 2 hours. Three washes with 1× PBS were performed and cells were fixed with 4% paraformaldehyde for 30 minutes, followed by blocking with Dako serum-free protein block (Agilent, X0909) for 1 hour. Platelets were stained with anti-CD62p (bs-0561R, Bioss, 1 : 80 dilution) and leukocyte were stained with anti-CD45 (ab10558, Abcam, 1 : 80 dilution) in Dako overnight. Five washes with 1× PBS were conducted and cells were then incubated with Goat anti-Rabbit IgG AlexaFluor 594 (R37117, Invitrogen, 1 : 1000 dilution) secondary antibody and Actin-Green 488 ReadyProbes (R37110, Invitrogen, 1 : 1000 dilution) conjugated antibody in Dako for 1.5 hours. Five more washes with 1× PBS were done and the coverslips were mounted to slides with ProLong Gold Antifade Mountant with DAPI (P36934, Invitrogen). Coverslips were imaged with confocal fluorescent microscopy and analyzed with ImageJ (NIH). Three images per coverslip and at least three coverslips per group were imaged and analyzed.

2.9. Characterization of dynamic clotting assay

Dynamic clotting assays were performed as previously described.[38,39] PDMS microfluidic devices were fabricated by combining SYLGARD 184 elastomer and curing agent (Dow) in a 10 : 1 ratio onto a custom 3D-printed mold and heat cured at 80 °C for 2 hours. Biopsy punches were used to form inlets and outlets on the devices, which were mounted onto glass slides using an adhesive (Loctite). Fibrinogen (2.5 mg mL^{-1}), 1× HEPES buffer, AlexaFluor 488 fibrinogen (Thermo Fisher; 0.05 μg mL^{-1}), and thrombin (Thermo Fisher; 0.5 U mL^{-1}) were combined into the clot reservoir, and the clot was allowed to polymerize for 2 hours. A flow buffer of fibrinogen (2.5 mg mL^{-1}), 1× HEPES buffer (Thermo Fisher), AlexaFluor 488 fibrinogen (0.01 μg mL^{-1}), and thrombin (0.1 U mL^{-1}) was flowed through the device at a flow rate of 10 μL min^{-1} to produce a shear rate of 10 s^{-1} for twenty minutes. Fluorescent images were taken with an EVOS Cell Imaging Systems microscope. Four devices per group were imaged and analyzed. All statistical analysis was performed using GraphPad Prism. Data containing two groups were analyzed using 2-tailed Student *t* tests. Data containing groups of three or more were analyzed using an ordinary 1-way ANOVA with a Tukey's *post hoc* test at a 95% confidence interval. $^{*}p < 0.05$, $^{**}p < 0.01$, $^{***}p < 0.001$, $^{****}p < 0.0001$.

3. Results

3.1. Liquid repellency and slipperiness

In this work, we fabricated four distinct surfaces – less slippery hydrophobic, more slippery hydrophobic, less slippery hydrophilic, and more slippery hydrophilic (Fig. 1). We fabricated less slippery hydrophobic surfaces by grafting heptadecafluoro-1,1,2,2-tetrahydrodecyl trichlorosilane (FDTCS) onto glass coverslips *via* vapor phase silanization. The low surface energy of the fluorocarbons resulted in hydrophobicity and the rigid, long-chain fluorocarbon backbone limited molecular mobility, resulting in lower slipperiness.[11,40] We fabricated more slippery hydrophobic surfaces by grafting 1,3-dichlorotetramethyldisiloxane (DCTMS) onto glass coverslips *via* vapor phase silanization. The low surface energy of the hydrocarbons resulted in hydrophobicity and inherent flexibility of siloxane brushes resulted in higher slipperiness. We chose untreated glass coverslips as the less slippery hydrophilic surfaces. The high surface energy of glass resulted in hydrophilicity and the inherent inhomogeneities of the glass coverslips resulted in lower slipperiness. We fabricated more slippery hydrophilic surfaces by grafting high surface energy 3-[methoxy(polyethyleneoxy)9-12] propyltrimethoxysilane (PEGS) onto glass coverslips *via* liquid-phase silanization. The high surface energy of the ethylene glycol groups resulted in hydrophilicity and the low physical and

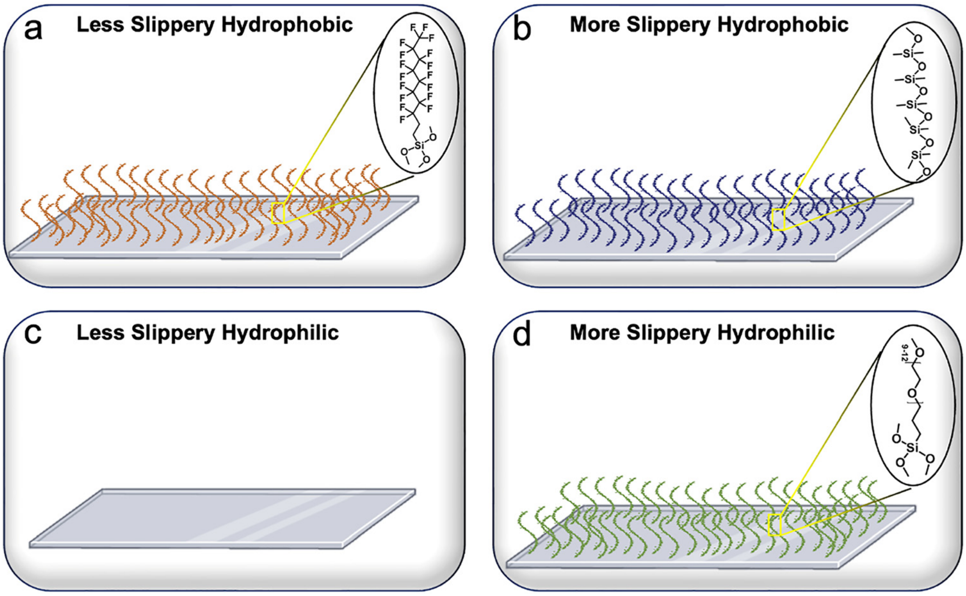

Fig. 1 Schematic illustration of different slippery surfaces. (a) Less slippery hydrophobic surfaces, (b) more slippery hydrophobic surfaces, (c) less slippery hydrophilic surfaces, and (d) more slippery hydrophilic surfaces.

chemical inhomogeneity of the PEGS brushes resulted in higher slipperiness.

We characterized the static contact angle (θ) and sliding angle (ω) using a contact angle goniometer with 20 μL water droplets (Fig. 2a and b; also see SI, Section 2). The less slippery hydrophobic surfaces displayed high static contact angles ($\theta \approx 105°$) and high sliding angles with ($\omega \approx 35°$), indicating high liquid repellency and low slipperiness. The more slippery hydrophobic surfaces displayed similarly high contact angles ($\theta \approx 102°$), but low sliding angles ($\omega \approx 8°$), indicating high liquid repellency and high slipperiness (Fig. 2a and b). The less slippery hydrophilic surfaces displayed low static contact angles ($\theta \approx 55°$) and high sliding angles ($\omega \approx 32°$), indicating low liquid repellency and low slipperiness. The more slippery hydrophilic surfaces displayed low contact angles ($\theta \approx 38°$) and low sliding angles ($\omega \approx 7°$), indicating low liquid repellency and high slipperiness (Fig. 2a and b). The experimentally measured sliding angles on all four surfaces align reasonably well with our theoretical estimations (see SI, Section 3). Droplet mobility measurements on a 40° inclined plane corroborated these trends, with more slippery surfaces exhibiting significantly higher sliding velocities than their less slippery counterparts under both hydrophobic and hydrophilic conditions (Fig. 2c–f). As anticipated, the water droplets moved slower on less slippery hydrophobic surfaces (average velocity $\approx$ 2.6 ± 0.7 mm s^{-1}; Fig. 2c) compared to more slippery hydrophobic surfaces (average velocity $\approx$ 13.6 ± 0.3 mm s^{-1}; Fig. 2d), and on less slippery hydrophilic surfaces (average velocity $\approx$ 1.3 ± 0.7 mm s^{-1}; Fig. 2e) compared to more slippery hydrophilic surfaces (average velocity $\approx$ 7.8 ± 0.2 mm s^{-1}; Fig. 2f). These results demonstrate that liquid repellency and slipperiness can be independently tuned.

3.2. Surface chemistry

We characterized the surface chemistry of all four surfaces using ATR-FTIR spectroscopy (Fig. 3a) after thoroughly rinsing the samples with isopropanol prior to analysis. Less slippery hydrophobic surfaces (FDTCS-grafted) exhibited C–H stretching vibrations at 2981 cm^{-1}, as well as CF_3 and CF_2 peaks at 1200 cm^{-1} and 1148 cm^{-1}, respectively, confirming the presence of fluorocarbon functional groups.[41,42] More slippery hydrophobic surfaces (DCTMS-grafted) displayed C–H stretching vibrations at 2962 cm^{-1} and 2855 cm^{-1}, along with Si–CH_3 peaks at 1260 cm^{-1} and 799 cm^{-1}, and Si–O–Si stretching at 1094 cm^{-1}, confirming the presence of hydrocarbon siloxane functional groups.[22,42] Less slippery hydrophilic surfaces (untreated glass) showed a dominant Si–O–Si peak at 1008 cm^{-1} characteristic of glass.[42] More slippery hydrophilic surfaces (PEG-silane grafted) exhibited broad O–H absorption bands around 3726 cm^{-1} and 3635 cm^{-1}, characteristic C–H stretching peaks at 2980 cm^{-1} and 2890 cm^{-1}, CH_2 bending at 1382 cm^{-1}, Si–C at 1253 cm^{-1}, C–O–C at 1156 cm^{-1}, and Si–O at 961 cm^{-1}, confirming the presence of PEGS groups.[43–45] We observed characteristic absorption bands corresponding to the functional groups of each surface chemistry, which remain evident even after isopropanol washing, confirming successful surface modification on the coverslip.

3.3. Surface topography

We characterized the surface roughness (R_{rms}) of all four surfaces using confocal laser scanning microscope (Fig. 3b). The contact angle hysteresis, and consequently surface slipperiness, are a function of the rigidity/flexibility of the molecules grafted to the surface as well as their physical homogeneity (*i.e.*, surface roughness) and chemical homogeneity. Among

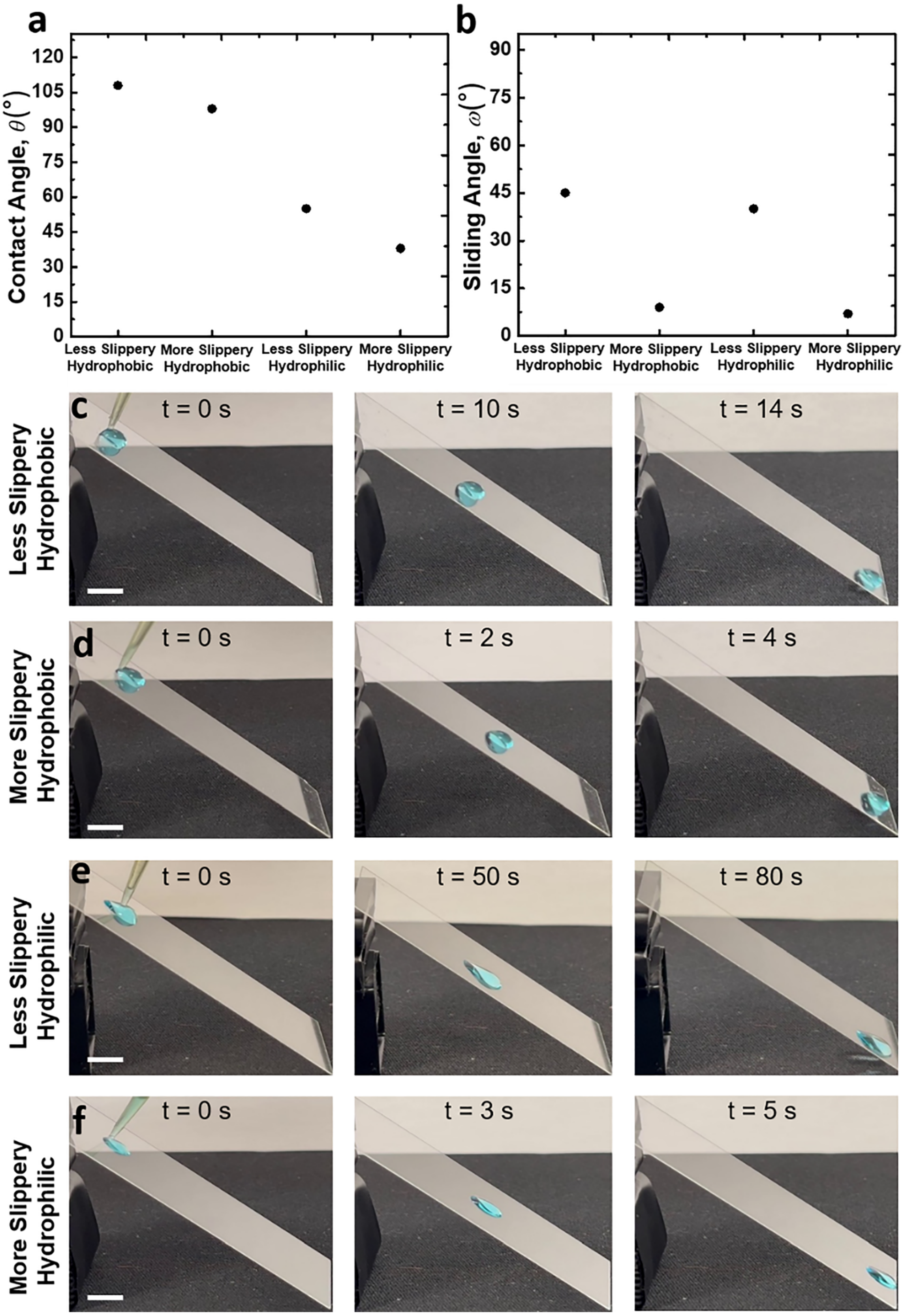

Fig. 2 Characterization of different slippery surfaces. (a), (b) Contact angle and sliding angle of water droplet on different slippery surfaces. (c)–(f) Series of images displaying the water droplet (20 μL) sliding at different slippery surfaces. Scale bar represents 1 cm.

hydrophobic surfaces, rigidity and high surface roughness ($R_{\text{rms}} \approx 2.2$ nm) of the fluorocarbon (FDTCS) molecules resulted in higher contact angle hysteresis (and consequently lower slipperiness); flexibility and lower surface roughness ($R_{\text{rms}} \approx 1.1$ nm) of the siloxane (DCTMS) molecules resulted in lower contact angle hysteresis (and consequently higher slipperiness). Among hydrophilic surfaces, we observed that the untreated coverslip, despite its lower surface roughness ($R_{\text{rms}} \approx 0.34$ nm), showed higher contact angle hysteresis (and consequently lower slipperiness), likely due to inherent chemical inhomogeneities. In contrast, we observed that more slippery hydrophilic surfaces, although exhibiting slightly higher roughness ($R_{\text{rms}} \approx 1.0$ nm), showed lower hysteresis and enhanced slipperiness, which we attribute to the flexibility and chemical homogeneity of the grafted PEGS molecules. Silanization process produces covalently bound, conformal

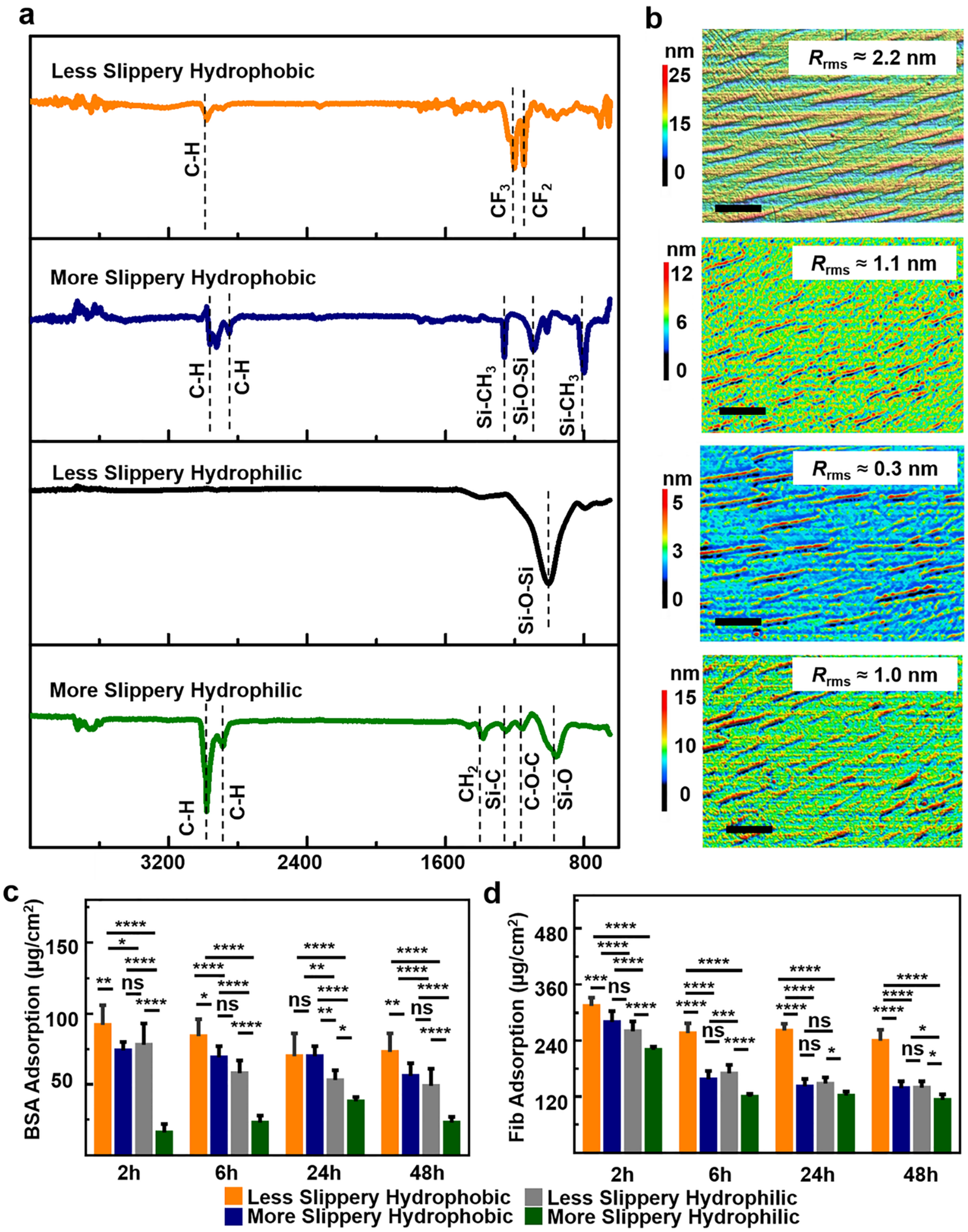

Fig. 3 Chemical characterization, surface topography, and protein adsorption. (a) ATR-FTIR spectra of all four surfaces confirming successful chemical functionalization. (b) Confocal laser scanning microscope images of all four surfaces showing surface topography. Scale bar represents 50 µm. (c), (d) Protein adsorption profiles of BSA and Fib on all four surfaces at different time intervals. ns-not significant, $^*p < 0.05$, $^{**}p < 0.01$, $^{***}p < 0.001$, $^{****}p < 0.0001$.

molecular layers that are typically a few nanometers thick.[19,44–49]

3.4. Solid surface energy

We estimated the solid surface energy of all four surfaces using the Owens-Wendt method. The surface energy of less slippery hydrophobic was $\Upsilon_{sv} \approx 12.4$ mN m^{-1}, and that of more slippery hydrophobic surface was $\Upsilon_{sv} \approx 20.2$ mN m^{-1}. In contrast, the surface energy of less slippery hydrophilic surface was $\Upsilon_{sv} \approx 38.2$ mN m^{-1}, and that of more slippery hydrophilic surface was $\Upsilon_{sv} \approx 62.6$ mN m^{-1}. The surface energy of hydrophobic surfaces is lower than that of hydrophilic surfaces because the hydrophobic surfaces are predominantly non-polar.[21,50–52]

3.5. Protein adsorption

We investigated protein adsorption kinetics of BSA and Fib on all four functionalized surfaces – less slippery hydrophobic, more slippery hydrophobic, less slippery hydrophilic, and more slippery hydrophilic (Fig. 3c and d). We observed that the highest amount of BSA adsorbed on less slippery hydrophobic surfaces at all time intervals, rising rapidly to a peak at 2 h (95 μg cm^{-2}) then plateauing by 24 h (75 μg cm^{-2}). The more slippery hydrophobic surfaces followed a similar trend but with intermediate adsorption levels, reaching 74 μg cm^{-2} at 2 h and decreasing to 56 μg cm^{-2} at 48 h. Among the hydrophilic substrates, the less slippery hydrophilic surfaces showed moderate adsorption that plateaued by 24 h (53 μg cm^{-2}). In contrast, on more slippery hydrophilic surfaces, we observed a gradual increase up to 24 h (40 μg cm^{-2}) followed by a decrease at 48 h (25 μg cm^{-2}). We observed similar trends for Fib, but at higher levels (110–320 μg cm^{-2}). The less slippery hydrophobic surfaces reached highest Fib, peaking at 2 h (310 μg cm^{-2}) and plateauing by 6 h (250 μg cm^{-2}). More slippery hydrophobic surfaces exhibited intermediate Fib adsorption, while substantially lower concentrations (120 μg cm^{-2}) adsorbed more slippery hydrophilic surfaces, plateauing by 6 h. Together, these results indicate that increased interfacial mobility plays a dominant role in reducing protein adsorption and facilitating dynamic protein exchange, even when surface energy considerations alone would predict greater adsorption.[50,53–55] This trend was consistently observed for both BSA and Fib, underscoring the role of slipperiness in regulating protein fouling on material surfaces.

3.6. Platelet adhesion and activation

Next, we examined the interactions of isolated human platelets with the various surfaces, coating glass coverslips with bovine serum albumin (BSA) as a negative control to reduce platelet adhesion and coating glass coverslips with fibrinogen (Fib) as a positive control since it is known for inducing platelet adhesion and activation. We isolated platelets from human whole blood, incubated them on all four surfaces, fixed the samples, and stained them using immunohistochemistry for actin and

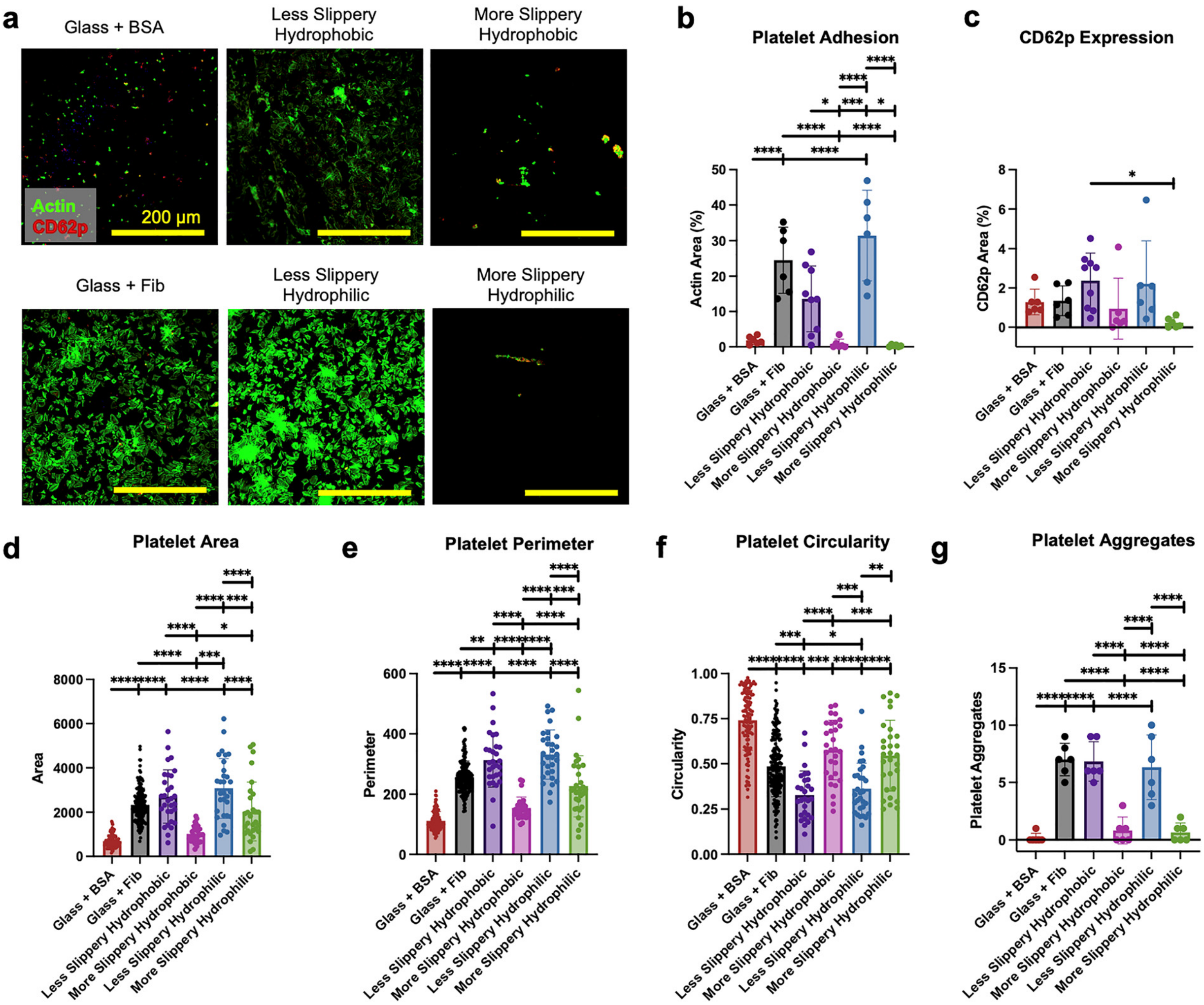

Fig. 4 Slippery surfaces reduce platelet adhesion and activation. (a) Representative immunofluorescent images of platelet adhesion and activation. Quantification of (b) area with platelet adhesion, (c) area with CD62p expression, (d) platelet area, (e) platelet perimeter, (f) platelet circularity, and (g) number of platelet aggregates. Six images were taken for each type of surface and at least ten platelets were measured in each image. $*p < 0.5$, $**p < 0.01$, $***p < 0.001$, $****p < 0.0001$.

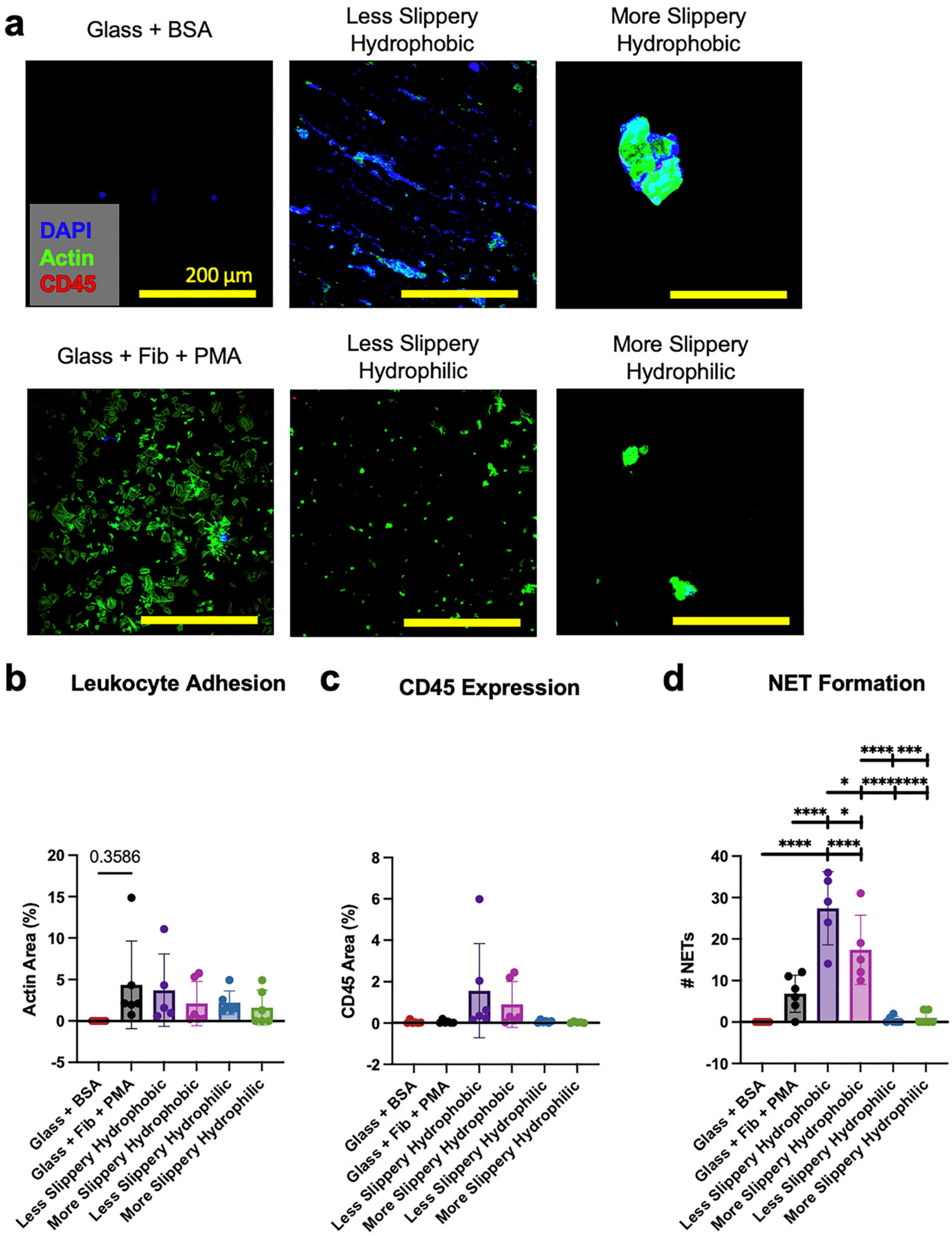

Fig. 5 Hydrophilic surfaces reduce white blood cell adhesion and activation. (a) Representative immunofluorescent images of leukocyte adhesion and activation. Quantification of (b) area with platelet adhesion and (c) area with CD45 expression. Six images were taken for each type of surface. $^*p < 0.5$, $^{**}p < 0.01$, $^{***}p < 0.001$, $^{****}p < 0.0001$.

CD62p. The surfaces were then imaged with a confocal microscope and analysis of the actin stain indicating platelet adhesion revealed that the positive control coverslips had significantly more platelets adhered than the negative control coverslips, as expected. Moreover, both the more slippery surfaces, regardless of hydrophilicity, had significantly reduced platelet adhesion (Fig. 4a and b). To measure platelet activation, platelets were stained with CD62p, also known as P-selectin, which has increased expression on platelet membranes and is also shed when platelets are activated. CD62p expression was similar between the positive and negative controls and only significantly reduced on the more slippery hydrophilic surfaces (Fig. 4a and c). When investigating additional parameters of platelet activation, the positive controls had significantly greater areas and perimeters than the negative controls. In addition, both of the more slippery surfaces had significantly reduced platelet area and perimeters indicating reduced platelet spread (Fig. 4d and e), significantly increased platelet circularity (Fig. 4f), and significantly fewer platelet aggregates (Fig. 4g) when compared to the less slippery surfaces, demonstrating reduced platelet activation. Altogether, our results indicate that slipperiness has a greater impact on platelet adhesion and activation than liquid repellency (hydrophobicity/hydrophilicity).

3.7. Leukocyte adhesion and activation

We investigated the effects of slipperiness and hydrophilicity on leukocyte adhesion and activation. As before, glass coverslips coated with BSA served as our negative control to reduce leukocyte adhesion. For our positive control, phorbol 12-myristate-13-acetate (PMA), a known activator of Protein Kinase C and neutrophil stimulant, was used;[38] glass coverslips were coated with Fib to facilitate leukocyte adhesion and PMA was added during leukocyte incubation. We isolated leukocyte from human whole blood, incubated them on all four surfaces, fixed the cells and stained for confocal imaging with immunohistochemistry for nuclei (DAPI), actin, and CD45 to identify leukocyte adhesion and activation. Analysis of actin staining showed that leukocyte adhesion was not significantly different among the different surfaces, even between the positive and negative controls (Fig. 5a and b). Lymphocytes and neutrophils account for the majority of leukocytes types, with approximately 20–40% of leukocyte composed of lymphocytes and approximately 40–60% of leukocyte composed of neutrophils on average. Because surfaces were incubated with all types of leukocytes from healthy human whole blood, we evaluated leukocyte activation based on indicators of lymphocyte and neutrophil activation. For lymphocyte activation, we performed immunofluorescent staining for CD45, a surface protein primarily expressed on lymphocytes and more highly expressed during lymphocyte activation. Though appearing mildly elevated on the hydrophobic surfaces, CD45 expression was not significantly different among the different surfaces, including the positive and negative controls (Fig. 5c). To quantify neutrophil activation, nuclei were stained with DAPI to identify neutrophil extracellular trap (NET) formation. Evaluation of NET formation revealed that neutrophil activation was significantly higher on hydrophobic surfaces, regardless of slipperiness (Fig. 5d). Therefore, hydrophilicity must be a critical consideration when designing materials to reduce leukocyte activation.

3.8. Clotting under flow conditions

Thus far, all assays were performed under static conditions. To better understand thrombosis under dynamic conditions, we used a custom microfluidics set-up.[38,39] We fabricated T-junction polydimethylsiloxane (PDMS) devices and mounted them onto glass slides that were either uncoated, which served as the less slippery hydrophilic surfaces, or grafted with PEGS brushes to be more slippery hydrophilic. A stationary clot containing fluorescent fibrinogen polymerized in the clot reservoir and an actively polymerizing flow buffer was flowed across the clot border at a flow rate mimicking physiologic

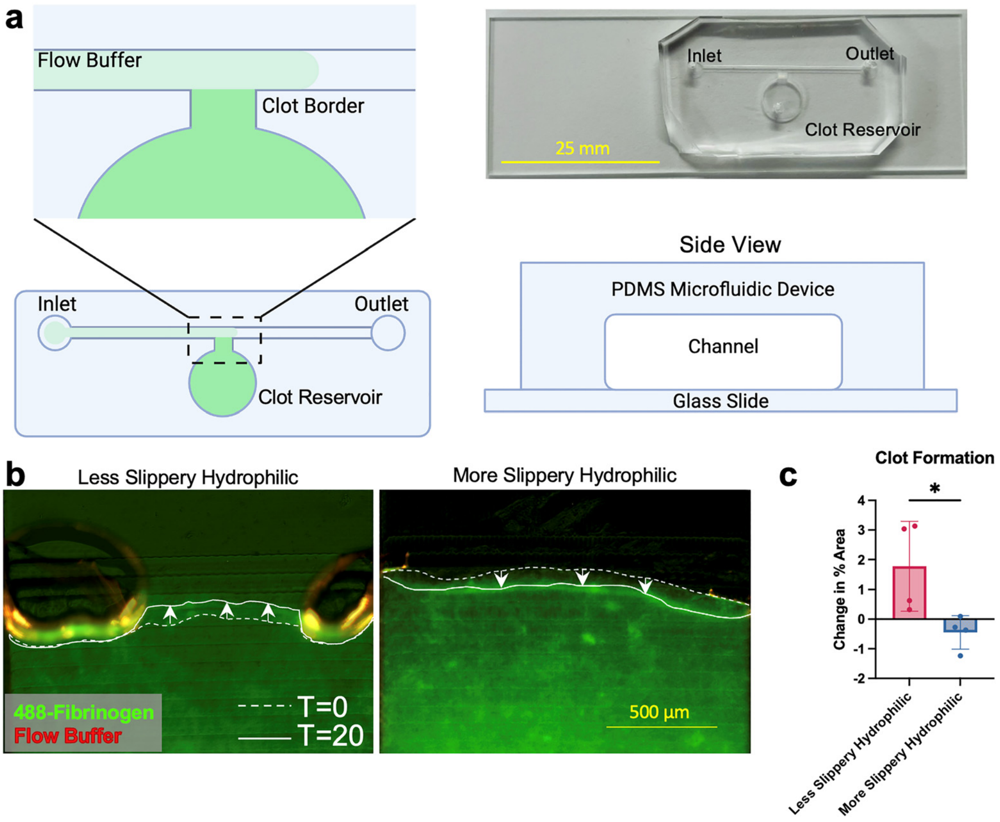

Fig. 6 A more slippery hydrophilic coating reduces clot formation on glass in a dynamic clotting assay. (a) Schematic of dynamic clotting assay. (b) Representative images of changes in clot borders on uncoated and more slippery hydrophilic-coated glass slides after twenty minutes of flow with a shear rate of 1 s^{-1}. (c) Quantification of changes in clot area over the course of twenty minutes. *$p < 0.05$.

venous shear rate of 10 s^{-1} (Fig. 6a). A venous shear rate was chosen, as opposed to an arterial shear rate, to better examine the effects of the surface coating, rather than mechanical flow. On uncoated glass slides, we observed that the clot border grew over 20 minutes, whereas on PEGS-coated glass slides, the clot border shrank. (Fig. 6b and c). Therefore, the more slippery hydrophilic coated glass surfaces not only inhibited clot formation but also facilitated clot regression. This regression could be due to physical shearing or promotion of degradation; however, further studies are needed to better understand the mechanisms at play.

4. Discussion and conclusion

More slippery hydrophilic surfaces hold great promise for the development of anti-thrombotic blood-contacting medical devices. While the present work does not directly quantify molecular-scale forces and is phenomenological in nature, the systematic decoupling of liquid repellency and surface slipperiness across well-defined surface chemistries provides a physical framework for interpreting the role of slipperiness in modulating blood-material interactions. However, the present study does have limitations. Firstly, the criteria of slipperiness were determined based on the sliding angles of water and not a more physiologically relevant solution. Future measurements using saline, plasma, or even whole blood will enable more accurate criteria for identifying the optimal slipperiness. Secondly, this study was conducted in a manner that is intentionally agnostic to other surface factors. Future work must focus on a comprehensive study that includes the roles of surface mechanical properties, surface charge, surface chemistry and brush architecture in determining blood-material interactions. Thirdly, both the stationary clots and the flow buffer used for examining the effects of coatings on clot formation under dynamic conditions were simple buffered solutions with isolated human fibrinogen and thrombin, rather than plasma. Future studies that compare thrombotic potential with plasma and blood from healthy and pro-thrombotic individuals will enable better understanding.

Overall, we have demonstrated that the combination of hydrophilicity and slipperiness significantly reduces platelet and leukocyte adhesion, platelet and leukocyte activation, as well as clot formation. From a translational perspective, this work establishes a path towards next-generation antithrombotic coatings. We demonstrated that slipperiness can be achieved through a simple and scalable silanization approach, which offers a practical and durable pathway for engineering antithrombotic surfaces on blood-contacting medical devices such as catheters, stents and extracorporeal circulation systems.

Author contributions

All authors contributed to the execution of the research. A. K. K. and A. C. B. supervised the project and secured funding. H. J. C., A. R., R. R. & A. A. conducted experiments, analyzed data, and drafted the manuscript. All authors discussed results and revised the manuscript.

Conflicts of interest

The authors declare that they have no financial conflicts of interest.

Data availability

The data that supports the findings of this study are available in the manuscript.

Supplementary information (SI) is available. See DOI: https://doi.org/10.1039/d5tb02723c.

Acknowledgements

A.K.K gratefully acknowledges financial support under award 2245427 from the National Science Foundation, under awards R21EB033960 and R01HL166724 from the National Institutes of Health, and under award HT94252310663 from Congressionally Directed Medical Research Programs. H. J. C. received funding under award F30HL173962 from the National Institutes of Health. A. A. received funding under award 5T34GM131947 from the National Institutes of Health.

References

1 Z. Nawrat, *Adv. Biomed. Eng.*, 2009, 1–59.
2 S. Movafaghi, W. Wang, D. L. Bark, L. P. Dasi, K. C. Popat and A. K. Kota, *Mater. Horizons*, 2019, **6**, 1596–1610.
3 V. Leszczak and K. C. Popat, *ACS Appl. Mater. Interfaces*, 2014, **6**, 15913–15924.
4 I. H. Jaffer and J. I. Weitz, *Acta Biomater.*, 2019, **94**, 2–10.
5 I. H. Jaffer, J. C. Fredenburgh, J. Hirsh and J. I. Weitz, *J. Thromb. Haemostasis*, 2015, **13**, S72–S81.
6 M. C. Sin, S. H. Chen and Y. Chang, *Polym. J.*, 2014, **46**, 436–443.
7 E. A. Vogler and C. A. Siedlecki, *Biomaterials*, 2009, **30**, 1857–1869.
8 R. M. Sabino, K. Kauk, S. Movafaghi, A. Kota and K. C. Popat, *Nanomedicine*, 2019, **21**, 102046.
9 D. C. Leslie, A. Waterhouse, J. B. Berthet, T. M. Valentin, A. L. Watters, A. Jain, P. Kim, B. D. Hatton, A. Nedder, K. Donovan, E. H. Super, C. Howell, C. P. Johnson, T. L. Vu, D. E. Bolgen, S. Rifai, A. R. Hansen, M. Aizenberg, M. Super, J. Aizenberg and D. E. Ingber, *Nat. Biotechnol.*, 2014, **32**, 1134–1140.
10 C. Howell, A. Grinthal, S. Sunny, M. Aizenberg and J. Aizenberg, *Adv. Mater.*, 2018, **30**, 1802724.
11 A. M. Rather, S. Vallabhuneni, A. J. Pyrch, M. Barrubeeah, S. Pillai, A. Taassob, F. N. Castellano and A. K. Kota, *Nat. Commun.*, 2024, **15**, 3735.
12 W. Wang, H. Vahabi, S. Movafaghi and A. K. Kota, *Adv. Mater. Interfaces*, 2019, **6**, 1900538.

13 T. S. Wong, S. H. Kang, S. K. Y. Tang, E. J. Smythe, B. D. Hatton, A. Grinthal and J. Aizenberg, *Nature*, 2011, **477**, 443–447.

14 D. J. Sutherland, A. M. Rather, R. M. Sabino, S. Vallabhuneni, W. Wang, K. C. Popat and A. K. Kota, *ACS Sustainable Chem. Eng.*, 2023, **11**(6), 2397–2403.

15 X. Tian, T. Verho and R. H. A. Ras, *Science*, 2016, **352**, 142–143.

16 S. Peppou-Chapman, J. K. Hong, A. Waterhouse and C. Neto, *Chem. Soc. Rev.*, 2020, **49**, 3688–3715.

17 W. Wang, H. Vahabi, S. Movafaghi and A. K. Kota, *Adv. Mater. Interfaces*, 2019, **6**, 1900538.

18 S. Vallabhuneni, S. Movafaghi, W. Wang and A. K. Kota, *Macromol. Mater. Eng.*, 2018, **303**, 1800313.

19 D. F. Cheng, C. Urata, B. Masheder and A. Hozumi, *J. Am. Chem. Soc.*, 2012, **134**, 10191–10199.

20 C. Zhang, L. Li, J. Chen, Y. Yang, B. Zuo, J. Li and X. Wang, *J. Phys. Chem. C*, 2020, **124**, 12448–12456.

21 A. Y. Fadeev and T. J. McCarthy, *Langmuir*, 1999, **15**, 3759–3766.

22 Y. L. Chen, C. A. Helm and J. N. Israelachvili, *J. Phys. Chem.*, 1991, **95**, 109–179.

23 Z. Wang, S. Paul, L. H. Stein, A. Salemi, S. Mitra, Z. Wang, S. Paul, L. H. Stein, A. Salemi and S. Mitra, *Polymers*, 2022, **14**(1075), 1–17.

24 X. Wang, Z. Wang, L. Heng and L. Jiang, *Adv. Funct. Mater.*, 2020, **30**, 1902686.

25 H. Zhao, C. Anand Deshpande, L. Li, X. Yan, M. Jahidul Hoque, G. Kuntumalla, M. C. Rajagopal, H. Chan Chang, Y. Meng, S. Sundar, P. Ferreira, C. Shao, S. Salapaka, S. Sinha and N. Miljkovic, *ACS Appl. Mater. Interfaces*, 2020, **12**, 12054–12067.

26 J. Li, W. Xia, J. Li, G. Wang, X. Wang, Z. Mo, X. Chen and K. Zhang, *Adv. Opt. Mater.*, 2024, **12**, 2302311.

27 H. Jing, L. Zhang, R. Hao, L. Li, X. Wang, Y. Han, Q. Xiao, Z. Shi and J. Sun, *Adv. Funct. Mater.*, 2025, e19210.

28 N. Pereyra, K. Yu, J. Rogalski, T. O. Da Silva, P. Golesorkhi, M. Goldstein, D. V. Devine and J. N. Kizhakkedathu, *Adv. Healthcare Mater.*, 2025, **14**, 2501217.

29 Y. Li, R. Ji, Y. Li, J. Li and H. Chen, *Anal. Chem.*, 2024, **96**, 10434–10442.

30 L. C. Xu and C. A. Siedlecki, *Biomaterials*, 2007, **28**, 3273–3283.

31 M. Crago, A. Lee, T. P. Hoang, S. Talebian and S. Naficy, *Acta Biomater.*, 2024, **180**, 46–60.

32 H. Vahabi, S. Vallabhuneni, M. Hedayati, W. Wang, D. Krapf, M. J. Kipper, N. Miljkovic and A. K. Kota, *Matter*, 2022, **5**, 4502.

33 P. Kantam, V. K. Manivasagam, T. K. Jammu, R. M. Sabino, S. Vallabhuneni, Y. J. Kim, A. K. Kota and K. C. Popat, *Adv. Mater. Interfaces*, 2023, **11**(1), 1–8.

34 P. Kantam, V. K. Manivasagam, T. K. Jammu, R. M. Sabino, S. Vallabhuneni, Y. J. Kim, A. K. Kota and K. C. Popat, *Adv. Mater. Interfaces*, 2024, **11**, 2300564.

35 W. Wang, J. Sun, S. Vallabhuneni, B. Pawlowski, H. Vahabi, K. Nellenbach, A. C. Brown, F. Scholle, J. Zhao and A. K. Kota, *Mater. Horizons*, 2022, **9**, 2863–2871.

36 L. W. Schwartz and S. Garoff, *Langmuir*, 2002, **1**, 219–230.

37 K. Liu, M. Vuckovac, M. Latikka, T. Huhtamäki and R. H. A. Ras, *Science*, 2019, **363**, 1147–1148.

38 A. Sheridan, K. Nellenbach, S. Pandit, E. Byrnes, G. Hardy, H. Lutz, N. Moiseiwitsch, G. Scull, E. Mihalko, J. Levy and A. C. Brown, *ACS Nano*, 2024, **18**, 15517–15528.

39 E. P. Mihalko, M. Sandry, N. Mininni, K. Nellenbach, H. Deal, M. Daniele, K. Ghadimi, J. H. Levy and A. C. Brown, *Blood Adv.*, 2021, **5**, 613–627.

40 S. Movafaghi, M. D. Cackovic, W. Wang, H. Vahabi, A. Pendurthi, C. S. Henry and A. K. Kota, *Adv. Mater. Interfaces*, 2019, **6**, 1900232.

41 W. S. Y. Wong, *Nano Lett.*, 2019, **19**, 1892–1901.

42 A. Shaporenko, A. Ulman, A. Terfort and M. Zharnikov, *J. Phys. Chem. B*, 2005, **109**, 3898–3906.

43 N. Kohler, G. E. Fryxell and M. Zhang, *J. Am. Chem. Soc.*, 2004, **126**, 7206–7211.

44 M. Zhang, W. hu, C. M. Earhart, M. Tang, R. J. Wilson and S. X. Wang, *J. Appl. Phys.*, 2010, **107**, 09B325.

45 C. Barrera, A. P. Herrera, N. Bezares, E. Fachini, R. Olayo-Valles, J. P. Hinestroza and C. Rinaldi, *J. Colloid Interface Sci.*, 2012, **377**, 40–50.

46 S. Flink, F. C. J. M. Van Veggel and D. N. Reinhoudt, *J. Phys. Org. Chem.*, 2001, **14**, 407–415.

47 J. A. Howarter and J. P. Youngblood, *Langmuir*, 2006, **22**, 11142–11147.

48 Y. Han, D. Mayer, A. Offenhäusser and S. Ingebrandt, *Thin Solid Films*, 2006, **510**, 175–180.

49 R. G. Acres, A. V. Ellis, J. Alvino, C. E. Lenahan, D. A. Khodakov, G. F. Metha and G. G. Andersson, *J. Phys. Chem. C*, 2012, **116**, 6289–6297.

50 D. V. Antonov, A. G. Islamova and P. A. Strizhak, *Materials*, 2023, **16**, 5932.

51 J. B. Brzoska, I. Ben Azouz and F. Rondelez, *Langmuir*, 2002, **10**, 4367–4373.

52 C. H. Lee, N. Johnson, J. Drelich and Y. K. Yap, *Carbon N. Y*, 2011, **49**, 669–676.

53 E. A. Vogler, *Biomaterials*, 2012, **33**, 1201–1237.

54 F. Zhang, E. T. Kang, K. G. Neoh, P. Wang and K. L. Tan, *Biomaterials*, 2001, **22**, 1541–1548.

55 Z. Yang, J. A. Galloway and H. Yu, *Langmuir*, 1999, **15**, 8405–8411.